# Structure-based design of charge-conversional drug self-delivery systems for better targeted cancer therapy

# Structure-based design of charge-conversional drug self-delivery systems for better targeted cancer therapy

**Haijun Xiao[a,1], Yiping Guo[b,1] Hongmei Liuc, Yushi Liu[c], Yumin Wang[a], Changqing Li[b,d], Jaroslav Císař[a], David Škoda[a], Ivo Kuřitka[a], Li Guo[c,e*], Vladimír Sedlank[a,**]**

[a]*Centre of Polymer Systems, Tomas Bata University in Zlin, Zlin, 76001, Czech Republic*

[b]*Quantitative and Systems Biology Program, University of California, Merced, CA, 95343, USA*

[c]*School of Pharmacy, Chengdu University of Traditional Chinese Medicine, Chengdu, 611137, China*

[d]*Department of Bioengineering, University of California, Merced, CA, 95343, USA*

[e]*State Key Laboratory of Characteristic Chinese Medicine Resources in Southwest China, Chengdu University of Traditional Chinese Medicine, Chengdu, 611137, China¨*

** Corresponding author. School of Pharmacy, Chengdu University of Traditional Chinese Medicine, Chengdu, 611137, China.*

*** Corresponding author. Centre of Polymer Systems, Tomas Bata University in Zlin, Zlin, 76001, Czech Republic.*

*E-mail addresses: guoli@cdutcm.edu.cn (L. Guo), sedlarik@utb.cz (V. Sedlařík).*

**ABSTRACT**

Various design and fabrication strategies of carrier-based drug delivery systems have been quickly established and applied for cancer therapy in recent years. These systems contribute greatly to current cancer treatments but further development needs to be made to eliminate obstacles such as low drug loading capacity and severe side effects. To achieve better drug delivery, we propose an innovative strategy for the construction of easy manufactured drug self-delivery systems based on molecular structures, which can be used for the co-delivery of curcuminoids and all the nitrogen-containing derivatives of camptothecin for better targeted cancer therapy with minimized side effects. The formation mechanism investigation demonstrates that the rigid planar structures of camptothecin derivatives and curcuminoids with relevant leaving hydrogens make it possible for them to be assembled into nanoparticles under suitable conditions. These nanoparticles show stabilized particle sizes (100 nm) under various conditions and tunable surface charges which increase from around -10 mV in a normal physiological condition (pH 7.4) to +40 mV under acidic tumor environments. In addition, in vivo mice experiments have demonstrated that, compared to irinotecan (a derivative of camptothecin) itself, the co-delivered irinotecan curcumin nanoparticles exhibited significantly enhanced lung and gallbladder targeting, improved macrophage-clearance escape and ameliorated colorectal cancer treatment with an eradication of life-threatening diarrhea, bringing hope for better targeted chemotherapy and clinical translation. Lastly, the strategy of structure based design of drug self-delivery systems may inspire more research and discoveries of similar self-delivered nano systems for wider pharmaceutical applications.

*Keywords:* Irinotecan, Curcumin, Charge conversion, Self-delivery, Targeting therapy, Diarrhea

## 1. Introduction

Cancer is the second largest cause of death globally. Chemotherapy based on small molecules remains one of the most effective ways to fight against various cancers. For example, topotecan (**Fig. 1**a), a derivative of camptothecin, has been used for the treatment of ovarian cancer, cervical cancer and lung cancer, among which lung cancer causes the largest cancer-related death in 2018 (1.8 million deaths) and still remains the leading diagnosed malignancy in 2018 (2.1 million new cases). Irinotecan (**Fig. 1**a), another camptothecin derivative, has been used as the first-line treatment for colorectal cancer **[1]**, the third most commonly diagnosed malignancy (1.8 million new cases in 2018) causing the second largest number of cancer-related deaths (0.86 million deaths in 2018). These small molecular chemotherapeutic agents are usually intravenously injected into the body yielding systemic effects. This approach is especially advantageous when dealing with metastatic cancer but the concomitant challenge involves balancing the therapeutic effects of the drug with their undesirable side effects **[2]**.

Many approaches have been explored to minimize the adverse effects of drugs as well as to solve other problems, such as the poor water solubility of more than 80% of drug candidates **[3,4]**, including altering their chemical structures by covalently conjugating with hydrophilic moieties **[5,6]** and making advantages of various carriers **[7]**. Nevertheless, these newly introduced moieties or carriers themselves need vigorous trials before clinical use **[8]** and they usually display a more complicated path through the clinic **[9]**. Furthermore, the involute design and fabrication procedures of many nanomedicines become real obstacles in the practical industrial manufacture **[10-12].**

Camptothecin is a natural hydrophobic alkaloid with multiple conjugated aromatic rings and rigid planar structure **[13,14] (Fig. 1**e), allowing it to sustain the DNA/topoisomerase complex and subsequently result in cell death **[15]**. Due to the lone pairs, the nitrogen-containing camptothecin derivatives are industrially protonated by forming salts with relevant medicinal acids to further improve their water solubility and minimize the toxicity (**Fig. 1**b). However, one common problem for all the derivatives of camptothecin is that they undergo pH-dependent lactone hydrolysis to get pharmacologically inactive carboxylate forms which show little topoisomerase inhibitory activity **[16,17]**. Besides, these camptothecin derivatives also cause many side effects, such as the vascular discomfort due to the low pH value (pH 3.5) of their commercial injections and the severely life-threatening diarrhea **[18]**.

Curcuminoids (**Fig. 1**c) are linear diarylheptanoids extracted from Curcuma longa. They exhibit many pharmacological effects and have been reported to attenuate cell resistance **[19,20]**, ameliorate gastrointestinal toxicity **[21]**, protect heart tissue **[22]** and also possess antitumor activities **[23,24]**. However, the applications of curcuminoids are heavily limited due to their extremely poor water solubility.

So far, no nano formulations based on these two molecular species have been reported. For the first time, we propose a strategy for the construction of easy manufactured drug self-delivery systems based on molecular structures, which can be used for the co-delivery of curcu-minoids and all the nitrogen-containing derivatives of camptothecin for better targeted cancer therapy via charge conversion. The formation mechanism investigation demonstrates that the two molecular species can self-assemble into complex of ion pairs in polar organic solvents through intermolecular non-covalent interactions, resulting in a uniform distribution with certain molar ratios before being penetrated into anti-solvents to form nanoparticles. As shown in **Scheme 1**, these nanoparticles show stabilized particle sizes (100 nm) under various conditions and tunable surface charges which increase from around -10 mV in a normal physiological condition (pH 7.4) to +40 mV under acidic tumor environments.

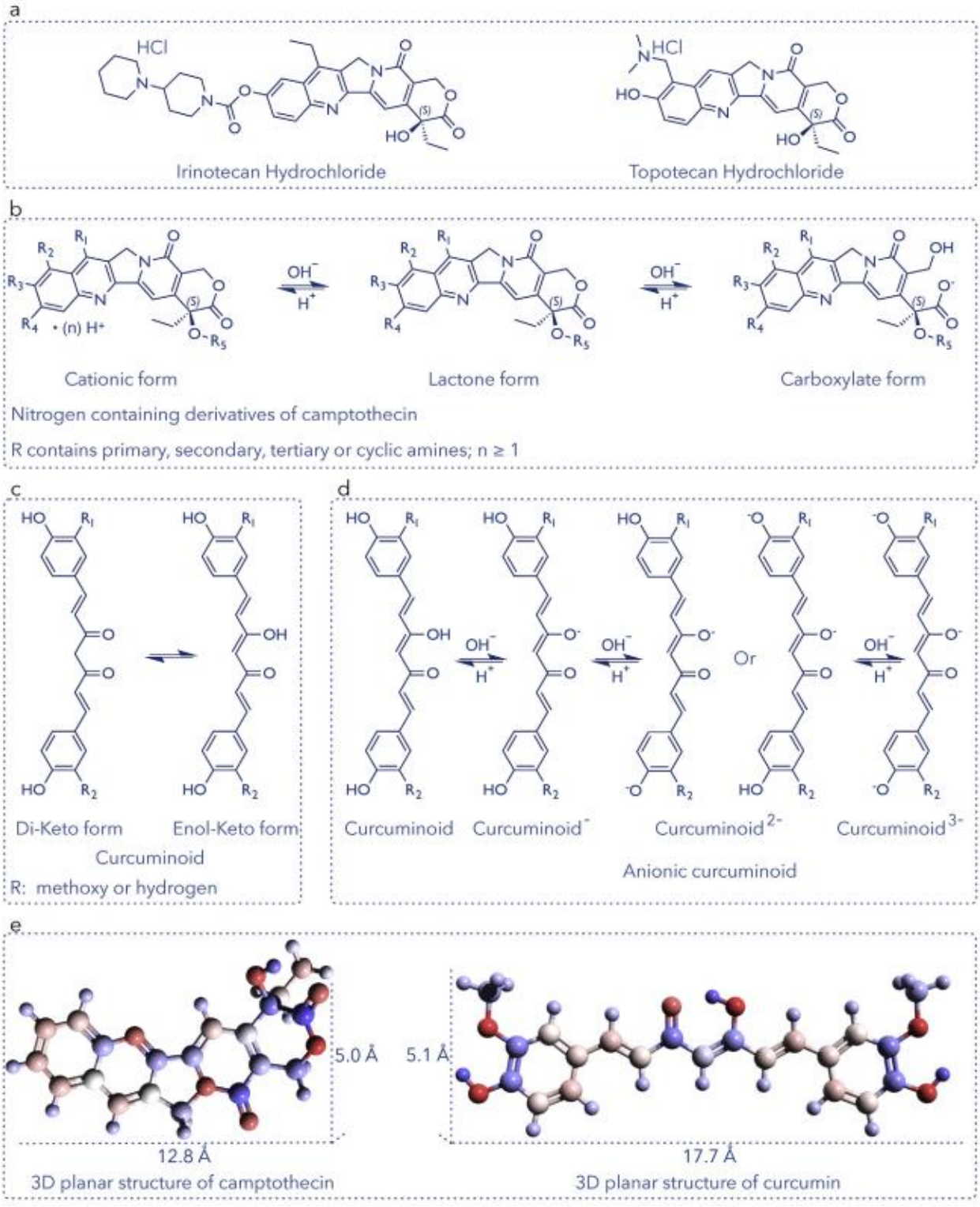


**Fig. 1.** Structures and properties of camptothecin derivatives and curcuminoids. (a) Chemical structures of irinotecan hydrochloride and topotecan hydrochloride. (b) Protonated nitrogen-containing derivatives of camptothecin by forming salts with medicinal acids (left); the pH-dependent lactone hydrolysis equilibria of camptothecin derivatives (right). (c) Chemical structures of curcuminoids in enol-keto tautomeric equilibria. (d) Dissociation equilibria between curcuminoids and their anions. (e) Three-dimensional grid planar structures and sizes of camptothecin and curcumin (color by partial charge; red, negative; blue, positive; Å, angstrom).

The water solubility of curcuminoids is dramatically improved and the lactone hydrolysis of camptothecin derivatives is also restricted to keep their pharmacologically active forms. Besides, the formulation with a pH value close to that of normal blood would reduce the side effects caused to blood vessels and improve the patient compliance compared to commercial injections of camptothecin derivatives (pH 3.5). More importantly, in vivo mice experiments have confirmed that, compared to irinotecan itself, the co-delivered ir-inotecan curcumin nanoparticles exhibited dramatically enhanced lung and gallbladder targeting, improved macrophage-clearance escape and better colorectal cancer treatment with an eradication of life-threatening diarrhea, which brings great hope for better targeted chemotherapy and clinical translation. The strategy of construction of drug self-delivery systems based on molecular structures may inspire more discoveries of similar formulations for wider pharmaceutical applications.

## 2. Materials and methods

### *2.1. Materials*

Irinotecan hydrochloride, topotecan hydrochloride, curcumin, po-loxamer 105, mannitol, glucose, paraformaldehyde and dimethyl sulfoxide (DMSO) were purchased from Sigma-Aldrich and used as received. Wortmannin, cytochalasin D, genistein and methyl-p-cyclodextrin were purchased from Meilun Biotechnology Co. Ltd (Dalian, China). Chlorpromazine was obtained from Selleck Chemicals (China). Phosphate buffered saline (PBS, pH = 7.4) was prepared in laboratory and ultrapure water was produced using a Milli-Q integral water purification system.

### *2.2. Nanoparticle preparation*

Surfactant stabilized irinotecan hydrochloride curcumin nanoparticles (SICN) were prepared based on a simple precipitation method. Briefly, irinotecan hydrochloride (6.2 mg) and curcumin (3.7 mg) (Molar ratio 1:1) were dissolved in dimethyl sulfoxide (DMSO, 300 pL), inside which 0.5 mg of injectable non-ionic surfactant poloxamer 105 was added.

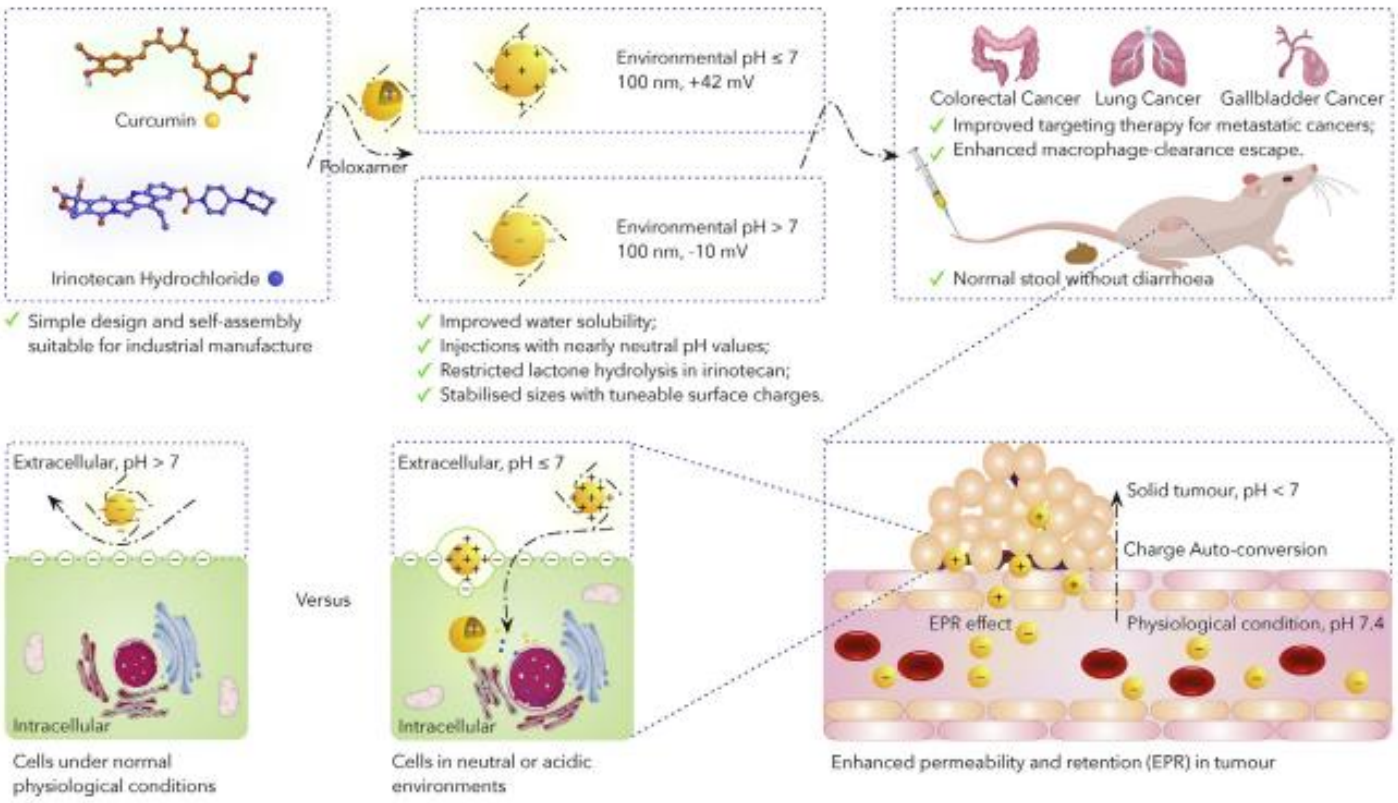


**Scheme 1.** Construction of charge-conversional drug self-delivery systems for better targeted cancer therapy.

The obtained organic solution was added into ultrapure water (30 mL) with magnetic stirring to get a suspension which was then dialyzed to remove the organic solvent. Nanoparticle powder was obtained after lyophilization with mannitol, which was then dispersed into ultrapure water containing glucose to get an injectable nanoparticle suspension.

Irinotecan hydrochloride curcumin nanoparticles without surfactants (ICN) and topotecan hydrochloride curcumin nanoparticles without surfactant (TCN) were also prepared using the same procedures.

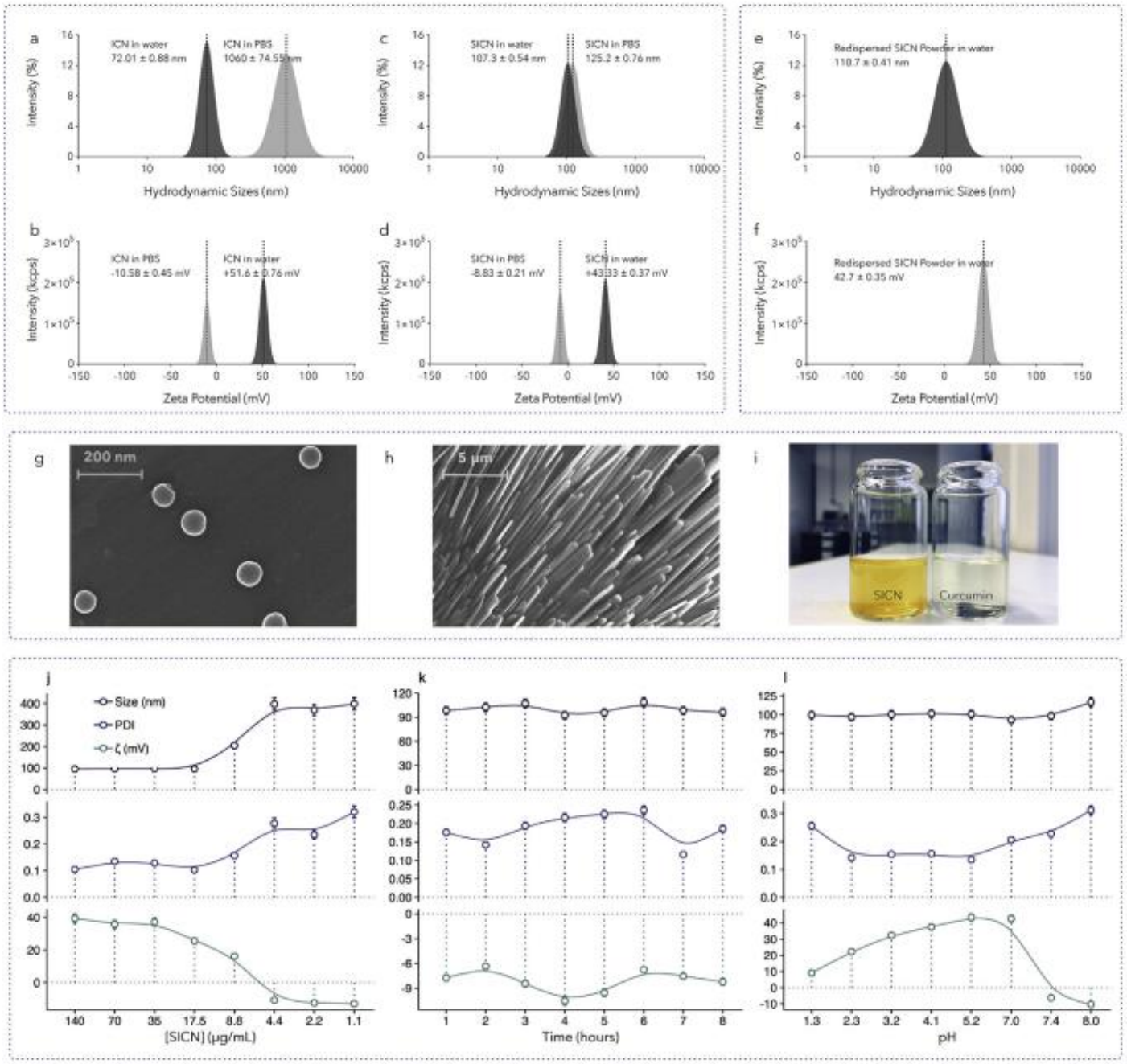


**Fig. 2.** Sizes, surface charges, redispersity, morphologies, appearance and stability of nanoparticles. (a) Particle sizes of ICN increase from about 70 nm in water to 1000 nm in PBS while (b) its surface charges decrease from 50 mV to -10 mV; (c) Stabilized particle sizes of SICN under various conditions; (d) Tunable surface charges of SICN increase from -7 mV in PBS (pH 7.4) to +41 mV in water; SICN powder shows easy redispersity with narrow size distribution (e) and strong surface charges (f); (g) Spherical SICN with smooth surfaces; (h) Morphology of lyophilized SICN with mannitol; (i) Apparent appearance of SICN and curcumin in water exhibits the dramatically improved water solubility of curcumin by forming nanoparticles with irinotecan hydrochloride. (j) Anti-dilution ability of SICN in water after serial dilution; (k) Storage stability of SICN in PBS at 37.5°C; (l) SICN shows stabilized sizes and distribution although its surface charges decrease with an increase of acidity in an acidic environment and the addition of alkaline buffer makes the surface charges become negative. < br > Tag as simple para: < br > Abbreviation: ICN: Irinotecan hydrochloride Curcumin Nanoparticles; SICN: Surfactant stabilized Irinotecan hydrochloride Curcumin Nanoparticles; PBS: Phosphate Buffer Saline, pH = 7.4.

*2.3. Nanoparticle characterization*

The hydrodynamic sizes and surface charges of nanoparticles in different conditions were characterized by dynamic light scattering (DLS). To investigate the morphologies of nanoparticles, a drop of nanoparticle water suspension was evaporated on an aluminum foil. All nanoparticles were coated with a thin layer of gold (conductive coating) before investigation under a scanning electron microscope (SEM). The diffraction and thermal behavior of nanoparticles were characterized by powder x-ray diffraction (PXRD) and differential scanning calorimetry (DSC), respectively.

*2.4. Fluorescence quenching*

The stock solution was prepared by dissolving 10 mg of irinotecan hydrochloride or curcumin into 10 mL of DMSO. The working solution was obtained by mixing 10 pL of irinotecan hydrochloride stock solution with different volumes (from 1 pL to 10 pL) of curcumin stock solution and the final volume was adjusted to 1 mL with DMSO. The fluorescence spectra and lifetime were recorded on a spectrophotometer (FL980, Edinburgh, England). The excitation and emission wavelengths were set at 385 nm and 428 nm, respectively. For fluorescence synchronous spectra, the emission off wavelength was 43 nm.

The working solution containing topotecan was prepared using the same method. The excitation and emission wavelengths were set at 395 nm and 433 nm, respectively. For fluorescence synchronous spectra, the emission off wavelength was 38 nm.

*2.5. Cells and mice*

HT-29 colorectal adenocarcinoma cells were obtained from Boster Biological Technology Co. Ltd (Wuhan, China). Male BALB/c nude mice, aged 5 weeks (18-22 g, SPF grade), were purchased from Dashuo experimental animals Co., Ltd. (Chengdu, China). All animal experiments were conducted under the guidelines approved by the Institutional Animal Care and Use Committee (IACUC) of Chengdu University of Traditional Chinese Medicine.

*2.6. In vivo therapeutic efficacy and biosafety*

HT-29 cell suspension (2 x $10^6$ cells per 200 µL) were subcutaneously injected into the flank of male BALB/c mice. When tumor volume reached around 100 mm3, the HT-29 tumor bearing nude mice were randomly divided into three groups (four or five mice for each group) and were intravenously injected with PBS, irinotecan hydrochloride (27.5 mg/kg/mouse) or SICN (equivalent irinotecan 27.5 mg/ kg/mouse) every other day for consecutive 20 days. Tumor volume was measured every third day and calculated according to the formula: Tumor volume = length x width$^2$/2. Mice were weighted every three days and the severity of diarrhea was scored according to the following standards **[25]**: 0 (normal, normal stool or absent); 1 (slightly wet and soft stool); 2 (moderate, wet and unformed stool with moderate perianal staining of the coat); and 3 (severe, watery stool with severe perianal staining of the coat). Mice were sacrificed after 5 days of medication discontinuation. Tumors were excised, weighted and photographed. The excised tissues (heart, liver, spleen, lung, kidney, brain and tumor) were fixed in 4% paraformaldehyde to prepare paraffin sections. Hematoxylin/eosin (H&E) staining was used for histological analysis.

*2.7. Ex vivo biodistribution*

Mice with subcutaneous tumors of around 100 $mm^3$ were intravenously injected with irinotecan hydrochloride or SICN (equivalent irinotecan 27.5 mg/kg/mouse). Fluorescence based visual distribution of drugs and their average signal on excised tissues were obtained on a FUSION FX7 live animal imaging system.

## 3. Results and discussion

*3.1. Stabilized particle sizes and tunable surface charges*

The hydrodynamic sizes and surface charges of ICN nanoparticles under various conditions are displayed in **Fig. 2**. As can be seen, by changing the solvent from water to PBS (pH 7.4), the particle sizes of ICN increase from about 70 nm to more than 1000 nm (**Fig. 2a**) while their surface charges decrease from around 50 mV to about -10 mV (**Fig. 2b**). Compared to ICN in water, the addition of injectable nonionic surfactant poloxamer 105 slightly increases the hydrodynamic sizes of SICN nanoparticles to around 100 nm (**Fig. 2**c) while slightly decreases their surface charges to about 40 mV in water (**Fig. 2**d). In addition, altering the solvent to PBS further decreases the surface charges of SICN to around —10 mV, while their hydrodynamic sizes keep almost the same due to the additional steric repulsion provided by the non-ionic surfactants **[26]**, making SICN become independent of environmental pH values and ionic strength.

The stabilized particle sizes and tunable surface charges can benefit the drug self-delivery system by ameliorating their biodistribution and enhancing their passively targeted cellular internalization. Nanoparticles with negative surface charges can be repulsed by the negatively charged cell membrane under normal physiological conditions, resulting in prolonged circulation times **[27,28]** and facilitating tumor accumulation via enhanced permeability and retention (EPR) effect **[29]**. While the positively charged nanoparticles under neutral or acidic environments become efficient at cell penetration, leading to an improved accumulation in acidic tumor tissues **[28]**. Besides, compared to the commercial irinotecan hydrochloride injection (pH 3.5), the injectable SICN suspension with a pH value close to that of normal blood would reduce the side effects caused to blood vessels during injection and improve the compliance of patients.

*3.2. Morphology and appearance*

The morphologies of evaporated SICN nanoparticles and their lyo-philized powder with mannitol were characterized by SEM. For the evaporated SICN, spherical particles with smooth surfaces are displayed in **Fig. 2**g and their sizes are similar to those in suspension (around 100 nm). The morphologies and sizes of evaporated SICN nanoparticles under environments with different pH values keep almost the same (**Figs. S1 and S2**), demonstrating the good stability of nanoparticle. After lyophilization with mannitol, from **Fig. 2**h, we have observed only rod-like crystalline mannitol. The apparent appearance of SICN and curcumin in water is shown in **Fig. 2**i. Compared to pure curcumin in water, the water solubility of curcumin is markedly improved by forming nanoparticles with irinotecan hydrochloride.

*3.3. Stability*

The stability of SICN nanoparticles under various conditions was characterized by DLS. As shown in Fig. 2j, the particle sizes, surface charges and size distribution of SICN change little even though the concentration is low to about 10 pg/mL in suspension, implying their strong anti-dilution ability. Besides, SICN can keep stable in PBS (pH 7.4) at 37.5 °C for 8 h (Fig. 2k) though their absolute surface charges are less than 10 mV. Besides, although the surface charges of SICN decrease with an increase of acidity in an acidic environment and the addition of alkaline buffer makes the surface charges become negative (Fig. 2l), the hydrodynamic sizes and size distribution of SICN stay the same with few changes. In addition, the size and surface charges of redispersed SICN powder in water (Fig. 2e and f) keep almost the same compared to those before lyophilization. All these results demonstrate the good stability and easy redispersity of SICN nanoparticles.

Fig. 3. Crystalline profiles of SICN nanoparticles and fluorescence quenching of irinotecan chloride in DMSO caused by curcumin. Physical mixture of irinotecan hydrochloride and curcumin (c, molar ratio 1:1) shows superimposed PXRD patterns of both irinotecan hydrochloride (a) and curcumin (b); vacuum dried powder of methanol solution containing irinotecan hydrochloride and curcumin (d, molar ratio 1:1) shows evident novel diffraction peaks; SICN (e) shows new peaks at 11.22°, 23.68°, 25.66°, 28.66° and 29.42° compared to its components including irinotecan hydrochloride (a), curcumin (b) and P105 (f). DSC profile of P105 (g) implies its amorphous state; DSC profile of irinotecan hydrochloride and curcumin mixture (h, ratio 1:1) indicates their amorphous state after cooling from high temperature; Melting point of SICN at 155.6°C (i). The fluorescence excitation (j, emission at 428 nm), emission (k, excitation at 385 nm), synchronous (l, emission off 43 nm) spectra and fluorescent lifetime (m, excitation at 385 nm, emission at 428 nm) of irinotecan hydrochloride (Iri) in presence of various amounts of curcumin (Cur) in DMSO at room temperature; (n) The Stern-Volmer plots for the fluorescence quenching of irinotecan hydrochloride at room temperature; (o) The plots of log (I < span data-format = "subscript" >0< /span >/I - 1) versus log(concentration of quencher (mol/L)). <br> Tag simple para as: <br> Abbreviation: PXRD, powder x-ray diffraction; DSC, differential scanning calorimetry; SICN, Surfactant stabilized Irinotecan hydrochloride Curcumin Nanoparticles; IR, instrumental response; DMSO, dimethyl sulfoxide; <br> Notes: I < span data-format = "subscript" >0< /span > and I represent the fluorescent intensity of irinotecan hydrochloride in the absence and presence of curcumin, respectively. t < span data-format = "subscript" >0< /span > and t represent the fluorescent lifetime of irinotecan hydrochloride in the absence and presence of curcumin, respectively.

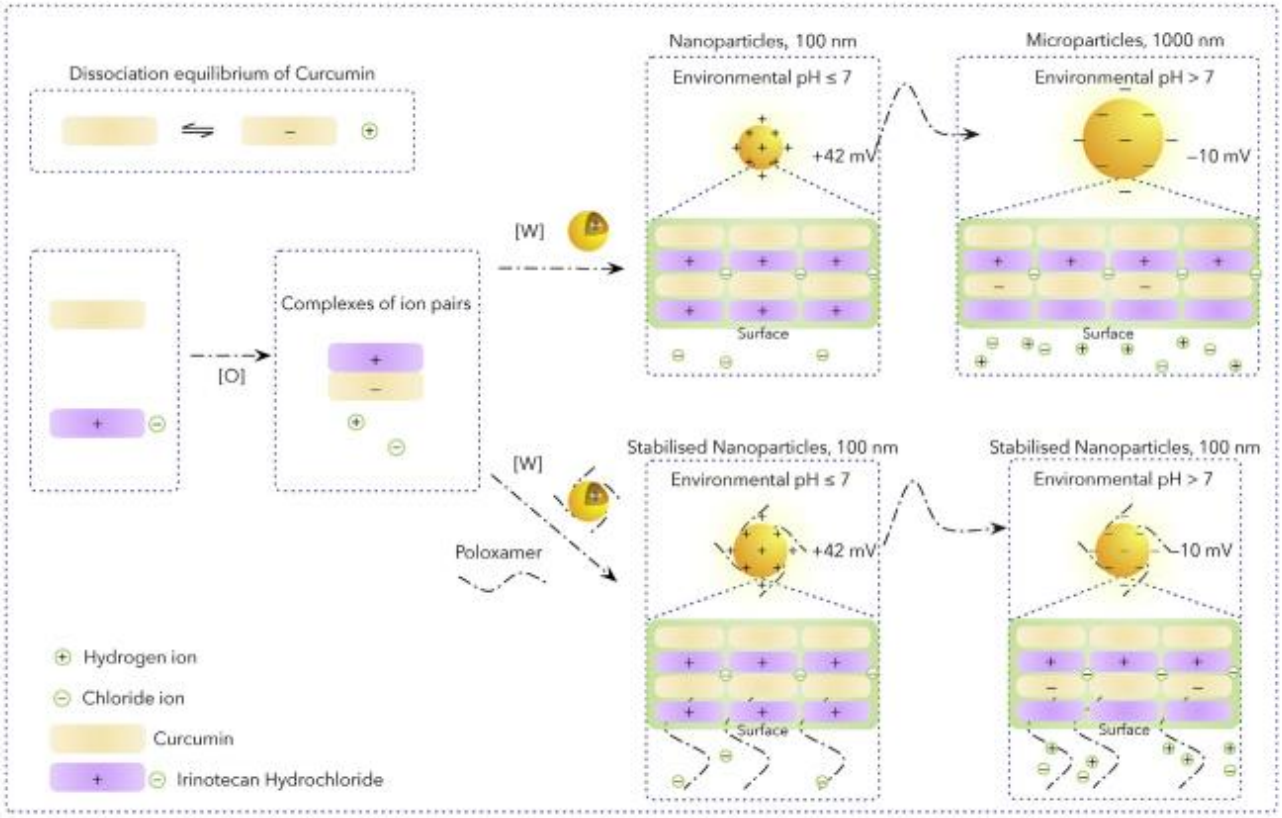


**Fig. 4.** Iillustration of the formation of surfactant stabilized irinotecan hydrochloride and curcumin nanoparticles. Irinotecan hydrochloride and curcumin initially self-assemble into homogeneous complexes of ion pairs in polar organic solvents. Nanoparticles are obtained by precipitation in presence of large volume of their unfavorable solvents regarding to the solubility. Surfactant stabilized nanoparticles become independent of environmental pH values and ionic strength because of the additional steric force provided by surfactants. < br > Tag as simple para: Abbreviation: [O], oil phase; [W], aqueous phase.

### *3.4. PXRD analysis*

The PXRD analysis of SICN and its components is displayed in Fig. 3. As can be seen, the physical mixture of irinotecan hydrochloride and curcumin with molar ratio 1:1 (Fig. 3c) shows superimposed diffraction patterns of both irinotecan hydrochloride (Fig. 3a) and curcumin (Fig. 3b). While the vacuum dried powder of methanol solution containing both irinotecan and curcumin (Fig. 3d) shows several evident novel diffraction peaks, indicating these two molecules are ordered in a new crystalline state with the help of methanol. SICN powder (Fig. 3e) shows new diffraction peaks at 11.22°, 23.68°, 25.66°, 28.66° and 29.42° compared to its components (Fig. 3a, b, and 3f), implying the formation of a novel crystal. By forming cocrystals, not only could the water solubility be improved (Fig. 2i), but the lactone hydrolysis in irinotecan is also restricted by the strong order effect of crystalline lattices.

### *3.5. Melting behavior*

The melting and crystallization behavior of SICN and its components were analyzed by DSC. In the DSC curves of surfactant poloxamer 105 (Fig. 3g), no evident endothermic or exothermic peaks appears in both the heating and cooling runs, indicating its amorphous state. In the second heating run of physical

mixture of curcumin and irinotecan hydrochloride (molar ratio 1:1, Fig. 3h), a glass transition occurs at about 140 °C, which implies that the mixture stays in an amorphous state after the first cooling from high temperature. However, there is a sharp endothermic peak at 155.6 °C in the heating run and an exothermic peak at 119 °C in the cooling run of SICN (Fig. 3i), which should be attributable to the melting and crystallization processes, respectively. The unique melting point of SICN at 155.6 °C also demonstrates they are in a crystalline form because an amorphous solid does not have a definite melting point.

*3.6. Static quenching*

The fluorescence excitation (Fig. 3j), emission (Fig. 3k), synchronous (Fig. 3l) spectra and fluorescent lifetime (Fig. 3m) of irinotecan hydrochloride in DMSO in the presence of various amounts of curcumin were measured by a fluorospectrometer at room temperature. Ir-inotecan hydrochloride shows an excitation maximum at 385 nm and an emission maximum at 428 nm. The addition of curcumin causes the fluorescence quenching in excitation, emission and synchronous spectra. However, the fluorescence lifetime of irinotecan hydrochloride keeps the same.

The fluorescence quenching data are analyzed by the Stern-Volmer equation [30]:

$$I_0/I = 1 + K_{sv} * [Q] = 1 + k_q * \tau_0 * [Q]$$

The binding number is calculated according to the following equation [30]:

$$\mathrm{Log}\,(I_0/I - 1) = \mathrm{Log}\,K_a + n * \log [Q]$$

where I0 and I represent the fluorescent intensity of irinotecan hydrochloride in the absence and presence of curcumin, respectively. Ksv is the Stern-Volmer quenching constant and Kq is the bimolecular quenching constant; t0 is the fluorescence lifetime of fluorophore in the absence of quencher. Ka is the association constant, n is the binding number and [Q] represents the concentration of quencher.

As shown in Fig. 3n, a linear Stern-Volmer plot and the unchanged fluorescence lifetime in the absence and presence of curcumin (Fig. 3m) reveals that the quenching of irinotecan hydrochloride in DMSO is caused by assembling into ground state complexes with curcumin (static quenching) [30] with a molar ratio of 1:1 (Fig. 3o) through intermolecular interactions, such as hydrophobic interactions, hydrogen bonding, n-n stacking [31] and electrostatic adsorption [32].

*3.7. Formation mechanism*

Based on all the evidence obtained, a possible formation process of the SICN nanoparticles is illustrated in Fig. 4. Curcumin and irinotecan hydrochloride self-assemble into complexes of ion pairs in polar organic solvents through intermolecular interactions. The extremely poor water-solubility of curcumin and camptothecin (the parent compound of irinotecan), the relatively exposed hydrogen atoms and the rigid planar structures (Fig. 1e) of both molecules with multiple conjugated aromatic rings [33-35] provide the possibility of hydrophobic interactions, hydrogen bonding and n-n stacking between these

two molecules [36], respectively. In addition, due to the active methylene hydrogen of p-diketones and two other phenolic hydrogen in curcumin, there are three pKa values for the dissociation of acidic protons in curcumin, namely 7.8, 8.5 and 9.0 (Fig. 1d) [36-38]. The partial ionization of weak acids in polar organic solvents [39] grants curcumin the opportunity to interact with cationic irinotecan which is protonated by forming salts with hydrochloride. In return, the electrostatic adsorption between cationic irinotecan and anionic curcumin promotes the dissociation of curcumin in polar organic solvents.

The organic solution of ionic complexes is then drop-wisely added into large volume of their unfavorable solvents regarding to the solubility to form nanoparticles by precipitation [40], during which the presence of water with pH values lower than the pKa of curcumin results in the shifts of curcumin dissociation equilibria towards the molecular form [38] and therefore leads to the positively charged surface of SICN nanoparticles. The high magnitudes of surface charges play a pivotal role during the formation of nanoparticles, which allows them to be repulsed from each other electrostatically and prevented from aggregation in suspension.

However, the positive surface charges attributed from the proto-nated irinotecan also result in the environmental pH sensitivity of the ICN nanoparticles (Fig. 2a). The relatively alkaline nano-environment deprotonates not only cationic irinotecan but also the weakly acidic curcumin molecules, therefore leading to the neutral irinotecan molecules and partially negatively charged curcumin (depending on the specific pH values of the environment) on the surface of nanoparticles (Fig. 2b). In addition, the high ionic strength in suspension compresses the electric double layer of the nanoparticles [41], further leading to the decrease of their surface charges. The relatively lower magnitudes of the surface charges decrease the electrostatic repulsion between nanoparticles, resulting in the failure in preventing their aggregation and subsequently obtaining microscale particles.

The introduction of non-ionic surfactant, which is partially hybridized inside SICN nanoparticles through hydrophobic interactions, not only will not interrupt the electrostatic interactions between ir-inotecan hydrochloride and curcumin during the formation of nanoparticles, but also provides an additional repulsive steric force to prevent their aggregation [41], making the particle size and distribution of SICN nanoparticles become independent of environmental pH values and ionic strength (Fig. 2c).

### *3.8. Mechanism verification*

The strategy for design of drug self-delivery systems based on the molecular structures of curcuminoids and camptothecin derivatives was verified by preparing topotecan hydrochloride curcumin nanoparticles (TCN) using the same method. As can be seen in Fig. 5a, TCN shows a hydrodynamic size of around 126 nm with a narrow size distribution (PDI 0.18) in water and they also have positive surface charges with large magnitudes (Fig. 5b). TCN also shows smoothly spherical structure (Fig. 5d). In addition, similar fluorescence quenching behavior (Fig. 5j, k and 5l) and lifetime decay (Fig. 5m) between topotecan hydrochloride and curcumin in DMSO were observed, revealing the static quenching between the two molecules.

The physical mixture of topotecan hydrochloride and curcumin (molar ratio 1:1, Fig. 5g) shows superimposed diffraction patterns of both topotecan hydrochloride (Fig. 5e) and curcumin (Fig. 5f). However, TCN shows novel diffraction peaks at 11.20°, 23.67°, 24.57, 25.66°, 28.66° and 29.44° (Fig. 5h), demonstrating the different crystal state of TCN. More interestingly, these patterns have the same diffraction angles with those of ICN nanoparticles (Fig. 5i), further verifying that molecules with the

same chemical skeletons of camptothecin and curcumin can form nanoparticles via the similar formation mechanism by utilizing this strategy. However, their dissimilar relative diffraction intensity (e.g., 24.57° and 29.44°) and different melting points (Fig. 5c) evince the divergent subtle structures in both nanoparticles and also indicate their different molecular composition and arrangements.

### *3.9. In vitro cytotoxicity, uptake efficiency and internalization pathways*

The in vitro cytotoxicity and fluorescence-based cellular uptake efficiency of SICN nanoparticles under various environmental pH values were explored on HT-29 cells.

As shown in Fig. S3, the half maximal inhibitory concentration (IC50) of irinotecan hydrochloride on cells under normal environment (pH 7.4) is 15.25 pM. The IC50 of SICN nanoparticles on cells with environmental pH of 7.8, 7.4 and 6.5 are 0.278 mg/mL, 0.112 mg/mL and 0.019 mg/Ml, equaling to 7.720 pM, 3.112 pM and 0.537 pM of irinotecan hydrochloride, respectively. Significant difference between groups at every dosage level is obtained ($p < 0.001$). Compared to the free irinotecan hydrochloride, the in vitro cytotoxicity of SICN is significantly improved by forming nanoparticles. Besides, the acidic environments could result in greater in vitro cytotoxicity of SICN on HT-29 cells than the alkaline condition because of the conversional positive surface charges of nanoparticles under tumor environments and the negative surface charges under normal physiological conditions.

The fluorescence-based cellular uptake of SICN nanoparticles under different environmental pH values are shown in Fig. S4. The blank group, namely cells under normal conditions without SICN nanoparticles, shows no fluorescence. For SICN groups, cells under acidic environments exhibit significantly stronger fluorescence than those in alkaline conditions ($p < 0.001$), demonstrating the higher uptake efficiency of SICN under tumor environments.

The cellular internalization pathways of SICN nanoparticles on HT-29 cells were also tested by confocal laser scanning microscopy (Fig. S5). From the statistical results, the cellular uptake of SICN nanoparticles is significantly blocked at 4 °C, suggesting an energy-dependent internalization. Moreover, the cellular uptake is not affected by the macropinocytosis inhibitors (cytochalasin D and wortmannin), but significantly inhibited by the clathrin-mediated endocytosis inhibitor (chlorpromazine) and the caveolin inhibitors (genistein and methyl-p-cyclodextrin), indicating the SICN particles are at nano scale during internalization because nano-sized particles (smaller than 500 nm) are mainly endocytosed though clathrin- and caveolin-mediated endocytic pathways while micro-sized particles are internalized via macro-pinocytosis [42,43]. Besides, as shown in Figs. S4 and S5, SICN nanoparticles are evenly distributed in the cytosol around the nucleus due to the caveolin-mediated endocytosis which can bypass lysosomes [43].

### *3.10. Nanoparticle disposition*

The plasma concentration-time profiles of free irinotecan hydrochloride and SICN nanoparticles are shown in Fig. S6. The plasma concentration for irinotecan hydrochloride group decreases by around 80% after 2 h while the concentration for SICN group still keeps at about 50% in plasma. Mice receiving a single injection of SICN nanoparticles achieve an obvious improvement in plasma concentration and exposure compared to free irinotecan, which is consistent with the previous report in literature [44].

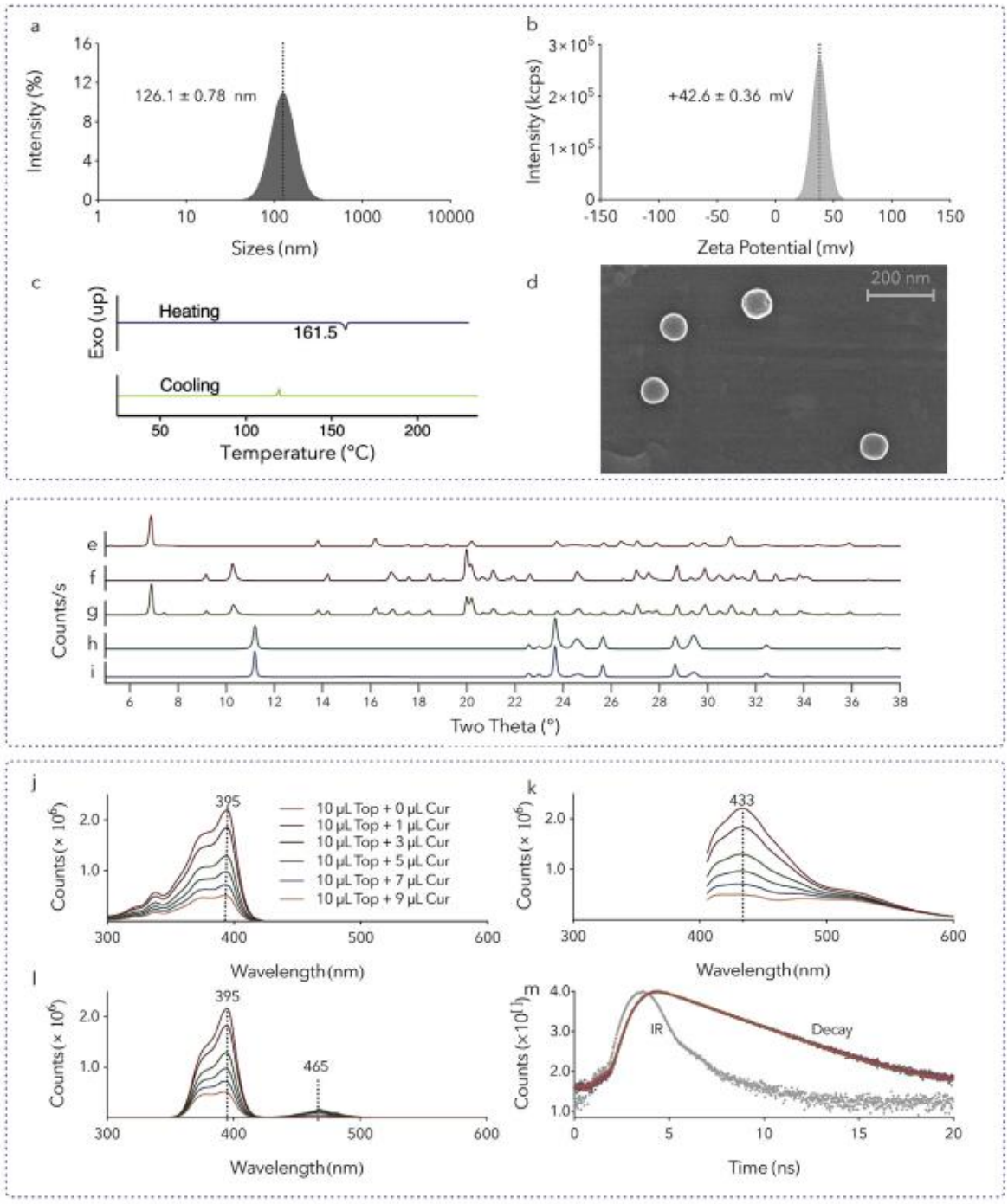


**Fig. 5.** Sizes, surface charges, morphologies and crystalline profiles of TCN nanoparticles and fluorescence quenching of topotecan hydrochloride in the presence of curcumin in DMSO. Typical hydrodynamic distribution (a) and surface charges (b) of TCN in water; (c) DSC profile of TCN shows its melting point at 161.5°C; (d) Smoothly spherical structure of evaporated TCN. Physical mixture of topotecan hydrochloride and curcumin (g, molar ratio 1:1) shows superimposed PXRD patterns of both topotecan hydrochloride (e) and curcumin (f); TCN (h, molar ratio 1:1) shows new peaks at 11.22°, 23.68°, 25.66°, 28.66° and 29.42° compared to its components including topotecan hydrochloride (e) and curcumin (f); TCN (h) and ICN (i) show similar diffraction patterns. The fluorescence excitation (j, emission at 433 nm), emission (k, excitation at 395 nm), synchronous (l, emission off 38 nm) spectra and fluorescent lifetime (m, excitation at 395 nm, emission at 433 nm) of topotecan hydrochloride (Top) in presence of various amounts of curcumin (Cur) in DMSO at room temperature. <br> Tag as simple para: <br> Abbreviation: PXRD, powder x-ray diffraction; DSC, differential scanning calorimetry; TCN, Topotecan hydrochloride Curcumin Nanoparticles; SICN: Surfactant stabilized Irinotecan hydrochloride Curcumin Nanoparticles. DMSO, dimethyl sulfoxide.

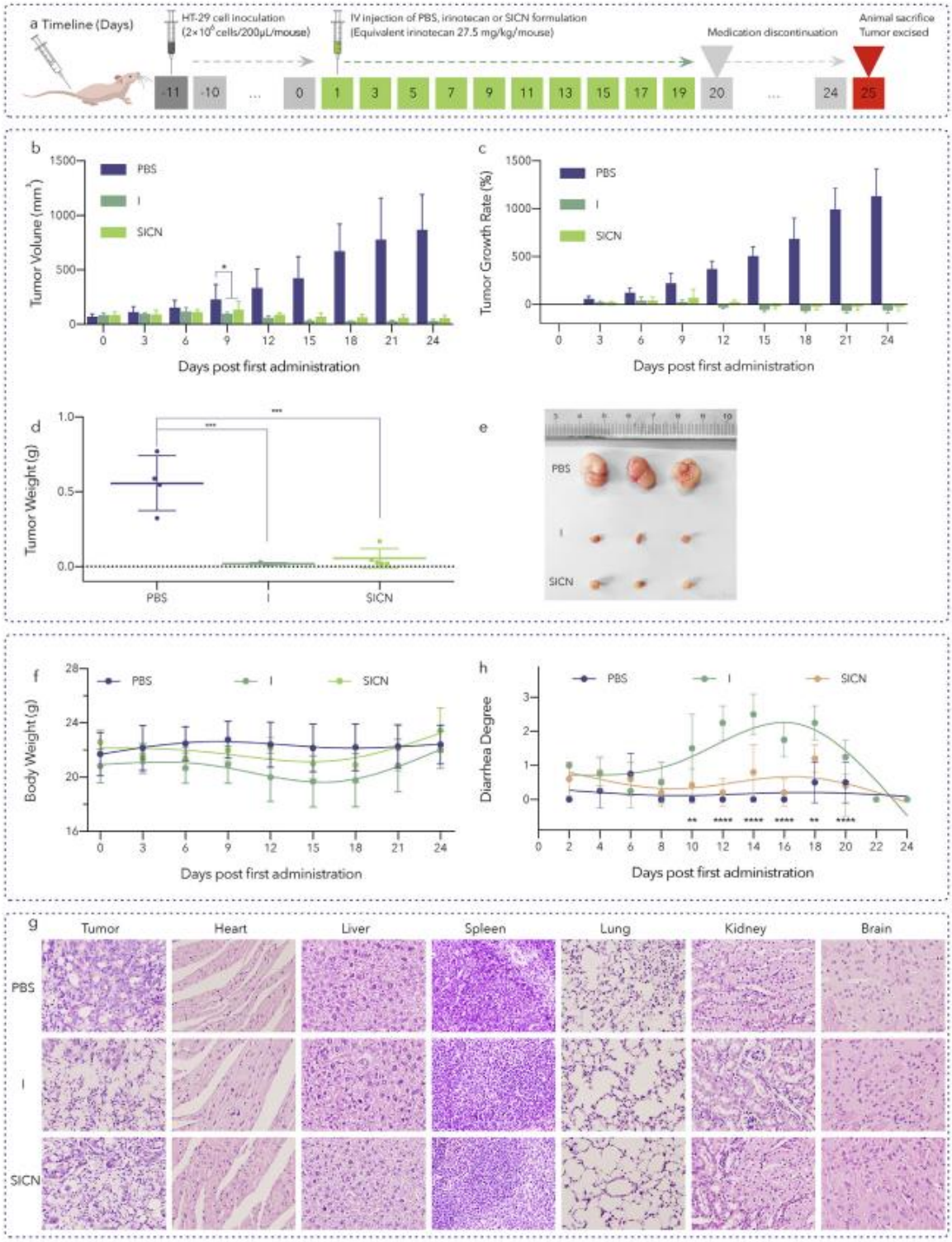


**Fig. 6**. < span data-format = "italic" > In vivo < /span > anticancer efficacy of SICN on HT-29 subcutaneous xenograft nude mice. (a) A schematic diagram of the experimental design of anticancer efficacy; (b) Tumor volume (b), tumor growth rate (c), tumor weight (d) and tumor images (e) from mice treated with PBS, I or SICN; (f) Negligible changes of Body weight; (g) H&E staining images of excised tumors and major organs (magnification of 400x). (h) Delayed diarrhea degree of mice (significant difference between SICN and I treated groups, no statistical difference between SICN and PBS treated groups). < br > Tag as simple para: < br > Abbreviation: IV, intravenous therapy; PBS, Phosphate buffered saline, pH 7.4; I, Irinotecan hydrochloride; SICN, Surfactant stabilized Irinotecan hydrochloride and Curcumin Nanoparticles. Significance of differences between groups are analyzed using 2way ANOVA. * p < 0.05, ** P < 0.01, *** P < 0.001, **** P < 0.0001.

*3.11. In vivo therapeutic efficacy and biosafety*

The anti-tumor effect of SICN nanoparticles was invested on HT-29 subcutaneous xenograft nude mice. The experimental strategy is illustrated in Fig. 6a. Compared to the PBS group, the average tumor volumes of mice in medication groups are effectively controlled and significant difference occurs on day 9 (around one week post first administration, Fig. 6b). The regression of tumor volume in the medication groups occurs on day 15 (around two week post first administration, Fig. 6c). The medication groups also show significant differences in tumor weight (Fig. 6d) and the photography of excised tumor is shown in Fig. 6e. No statistical difference between the two medication groups occurs during the whole experiment. These results confirm that the SICN nanoparticles is as equally effective in colorectal cancer treatment as free irinotecan hydrochloride and the tumor regression effect of SICN is caused by irinotecan instead of curcumin. This should be attributed to the significant difference in half maximal inhibitory concentration of the two molecules. Curcumin can be generally regarded as a biosafe molecule at the dose level.

No significant loss of body weight was observed in all the mice during the whole experiment, indicating the negligible side effects of the SICN nanoparticles for tumor therapy at the employed dose (Fig. 6f). Besides, the H&E staining images of tumors and major organs (heart, liver, spleen, lung, kidney and brain) from HT-29 tumor-bearing mice treated with PBS, free irinotecan or SICN are shown in Fig. 6g. Except for the glandular cavities, the H&E staining of colon cancer sections from the PBS group shows intact tumor cell structure. Cells exhibit distinct nuclei with a nearly spherical thin cytoplasmic region. H&E-stained sections of colon cancer from medication groups have distinct damage of tumor cell nuclei and distorted membranes surrounding necrotic tissues. However, compared to the PBS treated group, neither noticeable organ damage nor inflammation lesion can be observed in the medication groups, indicating the negligible organ dysfunction after being treated with SICN nanoparticles or irinotecan. All these results demonstrate that the SICN nanoparticles exhibit high biosafety for cancer treatment presenting no significant side effects to the treated mice.

As shown in Fig. 6h, significant delayed diarrhea in the mice treated with free irinotecan occurs on day 10 (10 days post first administration, $p < 0.01$) while no obvious diarrhea is observed in PBS or SICN treated group during the whole experiment, demonstrating the presence of curcumin in the nano formulation could protect the intestine and ameliorate the gut toxicity by alleviating diarrhea in mice. This can be due to whether the protective effects of curcumin molecule [21] or the formulation changes of irinotecan with the help of curcumin.

*3.12. Ex vivo biodistribution*

The ex vivo biodistribution investigation was carried out according to Fig. 7a. The normalized fluorescence spectra of irinotecan hydrochloride in water containing 50% of DMSO (Fig. 7b) and SICN in PBS (Fig. 7c) show that irinotecan in both forms display similar fluorescence behavior with an excitation maximum at around 370 nm and an emission maximum at about 430 nm.

The fluorescence based biodistribution of irinotecan hydrochloride and SICN on excised tissues are shown in Fig. 7d and e, respectively. Except for the high accumulation of irinotecan hydrochloride in tumor (Fig. 7d), a relatively higher biodistribution in liver can also be observed. Their relatively average signals are 27% and 37%, respectively (Fig. 7f). Compared to irinotecan hydrochloride, a visually higher accumulation of SICN in tumor is observed (Fig. 7e) and its relatively average signal figures prominently (36% in Fig. 7g, around 33% larger than that of free irinotecan, 27% in Fig. 7f), showing an improved tumor targeting of SICN. Besides, the relative accumulation of SICN in liver is lower (18% in Fig. 7g)

than that of free irinotecan (37% in Fig. 7f), which might also be one of the reasons that relieve the side effects. Clinically, the severe diarrhea caused by irinotecan hydrochloride is due to the biliary elimination and the subsequent micro-biome reactivation in intestines [45,46]. Therefore, except for the protective effect of curcumin on intestines [21], the diarrhea alleviation effect of SICN could also be attributable to the improved tumor targeting, which relatively reduces their quick accumulation in liver and lessens the chances of being rapidly metabolized and excreted into intestines.

To further verify this, the relative accumulation of irinotecan and SICN in tissues including heart, liver, gallbladder, spleen, lung, kidney, brain, tumor and stomach & intestine at different time post intravenous injection were explored in Fig. 7h. The relatively average signals of irinotecan are mainly distributed in liver, tumor and stomach & intestine. The relative accumulation in liver decreases from around 15% at 10 min to about 8% at 2 h post injection. The relative biodistribution in tumor increases from around 3%-12% while the relative accumulation in stomach & intestine keep at about 70%. However, except for the high accumulation in liver, tumor and stomach & intestine, high distribution of SICN in gallbladder and lung can also be observed. Compared to free irinotecan, the relative accumulation of SICN in liver and spleen decrease by around 50% during 30 min post injection (Fig. 7i), which could benefit the nanoparticles via escaping the rapid clearance by mononuclear phagocytic cells and prolonging their residence time in the body. Besides, their relative biodistribution in tumor increase by more than 50%, further evidencing their improved tumor targeting due to the uniform nano sizes (EPR effect) and convertible surface charges. In addition, their relative accumulation in stomach & intestine decrease by about 50%, which directly explains the diarrhea eradication effect of SICN. More interestingly, the relative accumulation of SICN in gallbladder and lung increase by two or more times. It shows significantly improved accumulation in lung and prolonged residence time in gallbladder, which not only explains the reduced accumulation in stomach & intestine but also brings hope for the treatment of lung and gallbladder cancer.

## 4. Conclusions

For the first time, we propose a strategy for the construction of drug self-delivery systems based on molecular structures, which can be used for the co-delivery of curcuminoids and all the nitrogen-containing derivatives of camptothecin for better targeted cancer therapy. The formation mechanism investigation demonstrates that these two molecular species can self-assemble into complex of ion pairs in polar organic solvents through intermolecular non-covalent interactions, resulting in a uniform distribution of them before being penetrated into anti-solvents to form nanoparticles. These nanoparticles show stabilized particle sizes (100 nm) with mono distribution (PDI < 0.2) under various conditions and conversional surface charges which increase from around —10 mV in a normal physiological condition (pH 7.4) to +40 mV under acidic tumor environments. The water solubility of curcuminoids is dramatically improved and the lactone hydrolysis of camptothecin derivatives is also restricted to keep their pharmacologically active forms. Besides, the formulation with a pH value close to that of normal blood would reduce the side effects caused to blood vessels and improve the patient compliance compared to commercial injections of camptothecin derivatives (pH 3.5). More importantly, in vivo mice experiments have demonstrated that, compared to irinotecan itself, the co-delivered irinotecan curcumin nanoparticles exhibited dramatically enhanced lung and gallbladder targeting, improved macrophage-clearance escape and ameliorated colorectal cancer treatment with an eradication of life-threatening diarrhea, exhibiting great promise for better targeted chemotherapy and clinical translation. Lastly, the strategy of structure based design of drug self-delivery systems may inspire more research and discoveries of similar self-delivered nano systems for wider pharmaceutical applications.

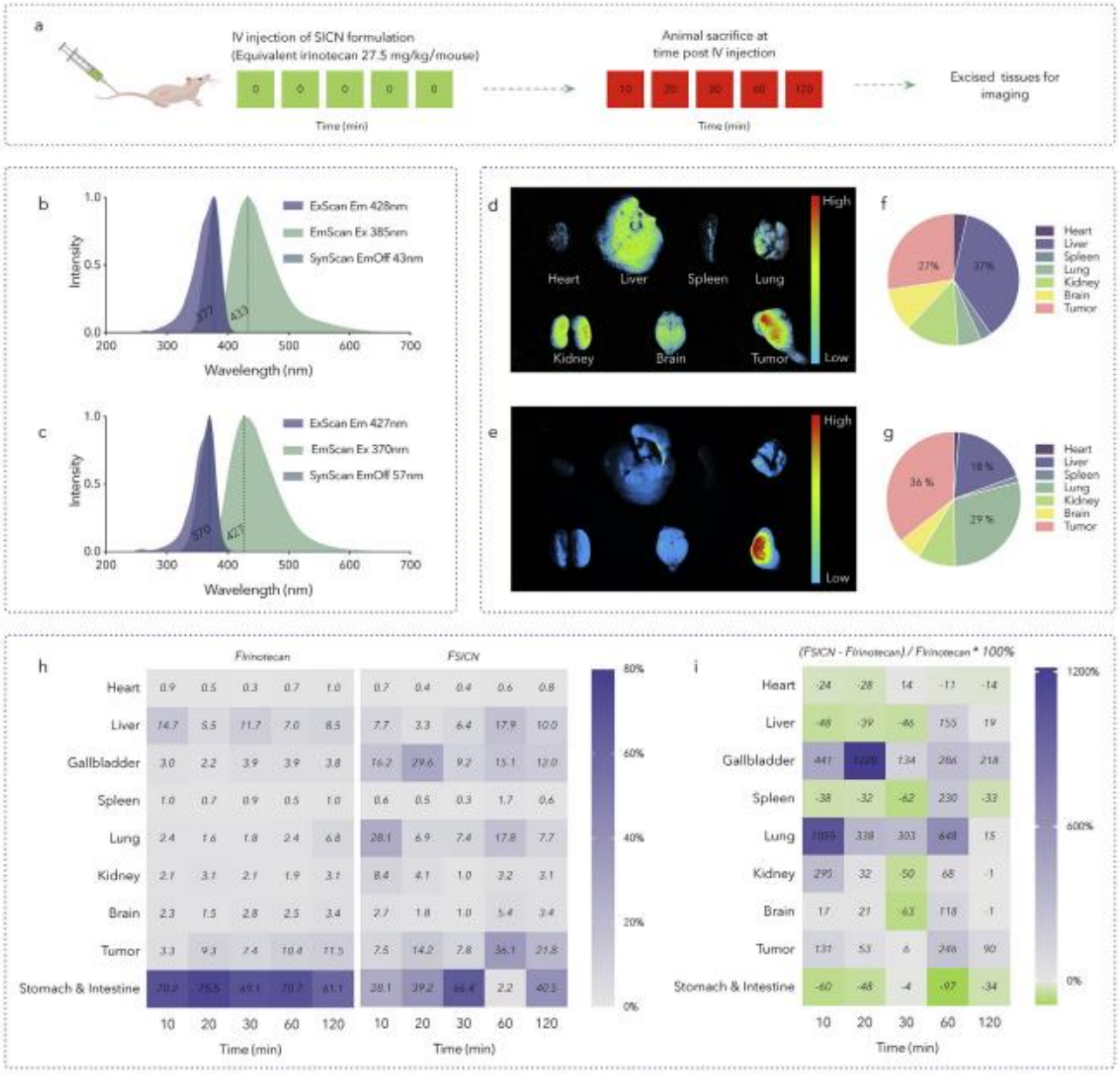


**Fig. 7.** < span data-format = "italic" > Ex < /span > < span data-format = "italic" > vivo < /span > distribution of SICN nanoparticles on HT-29 subcutaneous xenograft nude mice. (a) A schematic diagram of the experimental design of ex vivo biodistribution by using HT-29 tumor-bearing nude mice; Irinotecan hydrochloride in water containing 50% of DMSO (b) and SICN in PBS (c) exhibit similar behavior in their normalized fluorescence spectra; Fluorescence based relative biodistribution of irinotecan hydrochloride (d) and SICN nanoparticles (e) on tissues from mice sacrificed at 10 min post intravenous injection; The relatively average signal of irinotecan hydrochloride (f) and SICN nanoparticles (g) on excised tissues; (h) Heat map of relatively average signal of irinotecan and SCIN on tissues within 120 min post intravenous injection; (i) Heat map of relatively average signal increase rate of SICN compared to irinotecan within 120 min post intravenous injection. < br > Tag as simple para: < br > Abbreviation: PBS, Phosphate buffered saline, pH 7.4; SICN, Surfactant stabilised Irinotecan hydrochloride Curcumin Nanoparticles.

**Appendix A. Supplementary data**

Supplementary data to this article can be found online at https://doi.org/10.1016/j.biomaterials.2019.119701.

**References**

[1] W. Wulaningsih, A. Wardhana, J. Watkins, N. Yoshuantari, D. Repana, M. Van Hemelrijck, Irinotecan chemotherapy combined with fluoropyrimidines versus ir-inotecan alone for overall survival and progression-free survival in patients with advanced and/or metastatic colorectal cancer, Cochrane Database System. Rev. 2016 (2) (2016) CD008593-CD008593.

[2] V. Schirrmacher, From chemotherapy to biological therapy: a review of novel concepts to reduce the side effects of systemic cancer treatment (Review), Int. J. Oncol. 54 (2) (2019) 407-419.

[3] W. Wu, Y. Wang, K. Loebmann, H. Grohganz, T. Rades, Transformations between co-amorphous and co-crystal systems and their influence on the formation and physical stability of co-amorphous systems, Mol. Pharm. 16 (3) (2019) 1294-1304.

[4] T. Takagi, C. Ramachandran, M. Bermejo, S. Yamashita, L.X. Yu, G.L. Amidon, A provisional biopharmaceutical classification of the top 200 oral drug products in the United States, Great Britain, Spain, and Japan, Mol. Pharm. 3 (6) (2006) 631-643.

[5] M.K. Shim, J. Park, H.Y. Yoon, S. Lee, W. Um, J.-H. Kim, S.-W. Kang, J.-W. Seo, S.-W. Hyun, J.H. Park, Y. Byun, I.C. Kwon, K. Kim, Carrier-free nanoparticles of ca-thepsin B-cleavable peptide-conjugated doxorubicin prodrug for cancer targeting therapy, J. Control. Release 294 (2018) 376-389.

[6] A.G. Cheetham, R.W. Chakroun, W. Ma, H. Cui, Self-assembling prodrugs, Chem. Soc. Rev. 46 (21) (2017) 6638-6663.

[7] H. Cabral, K. Miyata, K. Osada, K. Kataoka, Block copolymer micelles in nanomedicine applications, Chem. Rev. 118 (14) (2018) 6844-6892.

[8] Y. Zhao, F. Fay, S. Hak, J.M. Perez-Aguilar, B.L. Sanchez-Gaytan, B. Goode, R. Duivenvoorden, C.d.L. Davies, A. Bjorkoy, H. Weinstein, Z.A. Fayad, C. Perez-Medina, W.J.M. Mulder, Augmenting drug-carrier compatibility improves tumour nanotherapy efficacy, Nat. Commun. 7 (1) (2016) 11221.

[9] V.J. Venditto, F.C. Szoka, Cancer nanomedicines: so many papers and so few drugs!, Adv. Drug Deliv. Rev. 65 (1) (2013) 80-88.

[10] R. Ghadi, N. Dand, BCS class IV drugs: highly notorious candidates for formulation development, J. Control. Release 248 (2017) 71-95.

[11] S.W. Morton, K.P. Herlihy, K.E. Shopsowitz, Z.J. Deng, K.S. Chu, C.J. Bowerman, J.M. DeSimone, P.T. Hammond, Scalable manufacture of built-to-order nanomedicine: spray-assisted layer-by-layer functionalization of PRINT nanoparticles, Advanced materials (Deerfield Beach, Fla, 25 (34) (2013) 4707-4713.

[12] K. Liu, Z. Zhu, X. Wang, D. Gonsalves, B. Zhang, A. Hierlemann, P. Hunziker, Microfluidics-based single-step preparation of injection-ready polymeric nanosystems for medical imaging and drug delivery, Nanoscale 7 (40) (2015) 16983-16993.

[13] J. Lopes-de-Araujo, S. Reis, C. Nunes, Topotecan effect on the structure of normal and cancer plasma membrane lipid models: a multi-model approach, Eur. J. Pharm. Sci. 123 (2018) 515-523.

[14] B.L. Staker, M.D. Feese, M. Cushman, Y. Pommier, D. Zembower, L. Stewart, A.B. Burgin, Structures of three classes of anticancer agents bound to the human topoisomerase I-DNA covalent complex, J. Med. Chem. 48 (7) (2005) 2336-2345.

[15] S.K. Das, I. Rehman, A. Ghosh, S. Sengupta, P. Majumdar, B. Jana, B.B. Das, Poly (ADP-ribose) polymers regulate DNA topoisomerase i (Top1) nuclear dynamics and camptothecin sensitivity in living cells, Nucleic Acids Res. 44 (17) (2016) 8363-8375.

[16] S. Palakurthi, Challenges in SN38 drug delivery: current success and future directions, Expert Opin. Drug Deliv. 12 (12) (2015) 1911-1921.

[17] T.Y. Ci, T. Li, G.T. Chang, L. Yu, J.D. Ding, Simply mixing with poly(ethylene glycol) enhances the fraction of the active chemical form of antitumor drugs of camptothecin family, J. Control. Release 169 (3) (2013) 329-335.

[18] F.N.U.A.U. Rahman, S. Ali, M.W. Saif, Update on the role of nanoliposomal ir-inotecan in the treatment of metastatic pancreatic cancer, Therap. Adv. Gastroenterol. 10 (7) (2017) 563-572.

[19] P. Su, Y. Yang, G. Wang, X. Chen, Y. Ju, Curcumin attenuates resistance to ir-inotecan via induction of apoptosis of cancer stem cells in chemoresistant colon cancer cells, Int. J. Oncol. 53 (3) (2018) 1343-1353.

[20] M. Murakami, S. Ohnuma, M. Fukuda, E.E. Chufan, K. Kudoh, K. Kanehara, N. Sugisawa, M. Ishida, T. Naitoh, H. Shibata, Y. Iwabuchi, S.V. Ambudkar, M. Unno, Synthetic analogs of curcumin modulate the function of multidrug resistance-linked ATP-binding cassette transporter ABCG2, Drug Metab. Dispos. 45 (11) (2017) 1166-1177.

[21] J.J. Johnson, H. Mukhtar, Curcumin for chemoprevention of colon cancer, Cancer Lett. 255 (2) (2007) 170-181.

[22] O. Ciftci, N.B. Turkmen, A. Taslidere, Curcumin protects heart tissue against ir-inotecan-induced damage in terms of cytokine level alterations, oxidative stress, and histological damage in rats, Naunyn Schmiedeberg's Arch. Pharmacol. 391 (8) (2018) 783-791.

[23] M.C. Bonferoni, S. Rossi, G. Sandri, F. Ferrari, Nanoparticle formulations to enhance tumor targeting of poorly soluble polyphenols with potential anticancer properties, Semin. Cancer Biol. 46 (2017) 205-214.

[24] J. Adiwidjaja, A.J. McLachlan, A.V. Boddy, Curcumin as a clinically-promising anticancer agent: pharmacokinetics and drug interactions, Expert Opin. Drug Metabol. Toxicol. 13 (9) (2017) 953-972.

[25] A. Kurita, S. Kado, N. Kaneda, M. Onoue, S. Hashimoto, T. Yokokura, Modified irinotecan hydrochloride (CPT-11) administration schedule improves induction of delayed-onset diarrhea in rats, Cancer Chemother. Pharmacol. 46 (3) (2000) 211-220.

[26] B. Sinha, R.H. Muller, J.P. Moschwitzer, Bottom-up approaches for preparing drug nanocrystals: formulations and factors affecting particle size, Int. J. Pharm. 453 (1) (2013) 126-141.

[27] W.W. Wang, X.Y. Li, Z.H. Wang, J.F. Zhang, X. Dong, Y.Z. Wu, C. Fang, A.W. Zhou, Y.L. Wu, A novel "mosaic-type" nanoparticle for selective drug release targeting hypoxic cancer cells, Nanoscale 11 (5) (2019) 2211-2222.

[28] F. Zhao, Y. Zhao, Y. Liu, X.L. Chang, C.Y. Chen, Y.L. Zhao, Cellular uptake, intracellular trafficking, and cytotoxicity of nanomaterials, Small 7 (10) (2011) 1322-1337.

[29] F. Meng, Z. Zhong, J. Feijen, Stimuli-responsive polymersomes for programmed drug delivery, Biomacromolecules 10 (2) (2009) 197-209.

[30] J.R. Lakowicz, Principles ofFluorescence Spectroscopy, Springer Science & Business Media, 2013.

[31] H.M. Su, H.M. He, Y.Y. Tian, N. Zhao, F.X. Sun, X.M. Zhang, Q. Jiang, G.S. Zhu, Syntheses and characterizations of two curcumin-based cocrystals, Inorg. Chem. Commun. 55 (2015) 92-95.

[32] D. Ke, Q.Q. Yang, M.L. Yang, Y. Wu, J.B. Li, H.B. Zhou, X.Y. Wang, Effect of the spacer length on the electrostatic interactions of cationic gemini surfactant micelles with trianionic curcumin, Colloids Surf., A 436 (2013) 80-86.

[33] P.P.N. Rao, T. Mohamed, K. Teckwani, G. Tin, Curcumin binding to beta amyloid: a computational study, Chem. Biol. Drug Des. 86 (4) (2015) 813-820.

[34] Y.C. Pommier, A foot in the door. Targeting the genome beyond Topoisomerase I with Camptothecins and novel anticancer drugs: importance of DNA replication, repair and cell cycle checkpoints, Curr. Med. Chem. Anti Cancer Agents 4 (2004) 429-434.

[35] S. Mourtas, M. Canovi, C. Zona, D. Aurilia, A. Niarakis, B. La Ferla, M. Salmona, F. Nicotra, M. Gobbi, S.G. Antimisiaris, Curcumin-decorated nanoliposomes with very high affinity for amyloid-^1-42 peptide, Biomaterials 32 (6) (2011) 1635-1645.

[36] E. Gazit, A possible role for pi-stacking in the self-assembly of amyloid fibrils, FASEB J. 16 (1) (2002) 77-83.

[37] H.H. T0nnesen, J. Karlsen, Studies on curcumin and curcuminoids - VI. Kinetics of curcumin degradation in aqueous solution, Z. Lebensm. Unters. Forsch. 180 (5) (1985) 402-404.

[38] W.-H. Lee, C.-Y. Loo, M. Bebawy, F. Luk, R.S. Mason, R. Rohanizadeh, Curcumin and its derivatives: their application in neuropharmacology and neuroscience in the 21st century, Curr. Neuropharmacol. 11 (4) (2013) 338-378.

[39] K. Sarmini, E. Kenndler, Ionization constants of weak acids and bases in organic solvents, J. Biochem. Biophys. Methods 38 (2) (1999) 123-137.

[40] S. Khan, M. de Matas, J.W. Zhang, J. Anwar, Nanocrystal preparation: low-energy precipitation method revisited, Cryst. Growth Des. 13 (7) (2013) 2766-2777.

[41] B.J. Palla, D.O. Shah, Stabilization of high ionic strength slurries using the

Dodělat 41